High-dimensional chaos from self-sustained collisions of solitons

O. Ozgur Yildirim[1,a)] and Donhee Ham[2,a)]
[1]*Cavium, Inc., 600 Nickerson Rd., Marlborough, Massachusetts 01752, USA*
[2]*Harvard University, 33 Oxford St., Cambridge, Massachusetts 02138, USA*

(Received 17 April 2014; accepted 11 June 2014; published online 20 June 2014)

We experimentally demonstrate chaos generation based on collisions of electrical solitons on a nonlinear transmission line. The nonlinear line creates solitons, and an amplifier connected to it provides gain to these solitons for their self-excitation and self-sustenance. Critically, the amplifier also provides a mechanism to enable and intensify collisions among solitons. These collisional interactions are of intrinsically nonlinear nature, modulating the phase and amplitude of solitons, thus causing chaos. This chaos generated by the exploitation of the nonlinear wave phenomena is inherently high-dimensional, which we also demonstrate. © *2014 AIP Publishing LLC*.
[http://dx.doi.org/10.1063/1.4884943]

Generation of chaotic dynamics in electronic media has been of pure and applied interest, and various ingenious chaotic circuits have been created, with a most notable example being Chua's circuit.[1–6] Since chaotic circuits can be constructed relatively easily—as compared to, for instance, optical or hydrodynamic chaotic systems—and their operation can be controlled in a facile, versatile manner, they represent a readily accessible experimental platform to emulate and interrogate chaotic behaviors that can occur in various other physical media. Chaotic circuits have also found such applications as random number generation[5] and chaotic communication.[6–8]

Adding to the repertoire of chaotic circuits, here we experimentally demonstrate another type of chaotic circuit. It is a self-excited, self-sustained chaotic oscillator, which combines, in a loop, an electronic amplifier and a nonlinear electromagnetic medium known as nonlinear transmission line (NLTL) [Fig. 1]. The NLTL creates voltage soliton pulses.[9–12] The amplifier provides gain to the solitons for their self-excitation and self-sustenance, but it also promotes collisions among the solitons, which is the key machinery behind our chaos generation. That is, we exploit the (self-sustained) physical nonlinear wave phenomena in attaining chaos.

Another key feature of our system lies in the *intrinsic* high-dimensionality of chaos it generates. The NLTL [Fig. 1] is an array of inductors and variable capacitors (varactors)—such as reverse-biased *pn*-junction diodes—whose capacitance varies with the voltage applied across them, thus, is nonlinear. Since a large number of these energy storage components comprise the NLTL, the chaos emerging from our *single* oscillator is intrinsically high-dimensional. This contrasts prior high-dimensional chaotic circuits[3,4] that are attained by coupling *multiple* low-dimensional chaotic subcircuits.

Chaotic oscillators utilizing spin wave solitons in magnetic films, optical solitons in fibers, and solitons in long Josephson junctions have been demonstrated.[13–15] Our chaotic soliton oscillator may be thought of as their electrical analogue. But, whereas the spin-wave and optical solitons are described by the nonlinear Schrödinger equation and the Josephson-junction solitons by the sine-Gordon equation, the NLTL solitons are governed by the Korteweg-de Vries (KdV) equation.[16,17]

To generate chaos, we promote collisions between solitons. Imagine two solitons with differing amplitudes traveling down the NLTL [Fig. 2(b)]. Since a taller soliton travels faster—this amplitude-dependent speed is one of key traits of solitons—the taller soliton catches up and collides with the shorter one. During the collision, the joint pulse assumes an amplitude not possible with linear superposition. After the collision, both solitons recover their original profile, but their positions are shifted from the positions expected in the absence of collisions[18] [see Fig. 2(b) vs. (a); d_1 is the position shift of the taller soliton due to collision]. These amplitude and position modulations born of collisions are responsible for our chaos generation.[19]

The amplifier can be designed to suppress or promote soliton collisions. A soliton traveling on the NLTL is always accompanied by small perturbations such as dispersive tails and noise. If the amplifier has a level-dependent gain, i.e., if it amplifies [attenuates] a signal above [below] a certain threshold (in analogy to saturable absorption in optics), the soliton is sustained—if its amplitude is larger than the threshold—while the small perturbations are suppressed [Fig. 3(a)]. Consequently, a stable periodic train of solitons (mode-locking) is observed in the time-domain voltage measurement at a node on the NLTL, as we experimentally demonstrated in prior work.[9–12] By contrast, if the amplifier offers full gain to all signal levels, the perturbations will grow out to form a small, parasitic soliton (or solitons) [Fig. 3(b)]. As this small parasitic soliton and the tall main soliton continue to circulate the loop at different speeds and keep colliding, their amplitudes and positions continue to be modulated, causing chaos. This was seen in our prior simulation work.[10,20] Experimental demonstration of this chaotic soliton oscillation is the goal of this work.

Before moving on to the experimental demonstration, we clarify that while in our system soliton collisions promoted by the amplifier generate chaos, in a pure KdV system—, e.g., a ring of idealized *lossless* NLTL *with no amplifier*—the dynamics involving soliton collisions do not

[a)]Authors to whom correspondence should be addressed. Electronic addresses: donhee@seas.harvard.edu and oozgury@gmail.com.

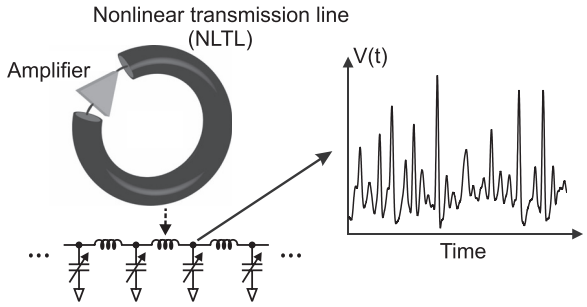

FIG. 1. Conceptual illustration of chaotic soliton oscillator.

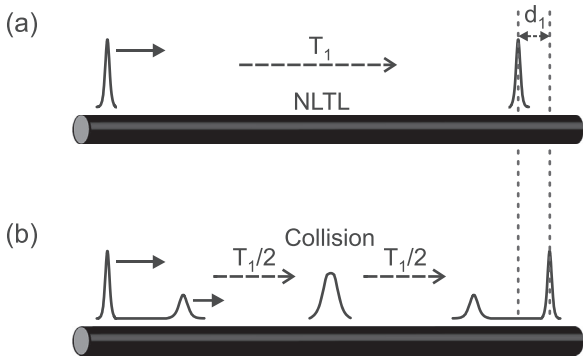

FIG. 2. Effects of soliton collision.

develop into chaos despite the phase and amplitude modulations the collisions cause; remarkably, it exhibits rather periodic behaviors such as the Zabusky-Kruskal recurrence.[17] This may be attributed to the complete integrability of the pure KdV system. But our system is not governed by the pure KdV equation due to the amplifier gain and NLTL loss, and thus is non-integrable; in this modified KdV system, chaos can arise from soliton collisions.[21] Thus, the cruciality of both the amplifier and NLTL soliton collision dynamics for our chaos generation is consistent with the formal consideration.

We first build a discrete oscillator that can produce both mode-locked and chaotic dynamics [Fig. 4(a)]. As we tune the amplifier characteristic from level-dependent gain to full gain, soliton collisions initially suppressed (which yields mode-locked soliton oscillation) are increasingly promoted, leading to chaotic oscillation. This dual-purpose circuit thus allows us to examine the collision-mediated route from stable to chaotic oscillation.

To tune the amplifier gain characteristic, we vary the resistance R_e, which sets the time constant of the R_eC_e network connected to the emitter of transistor $\mathbf{N}_1$ [Fig. 4(a)]. With a

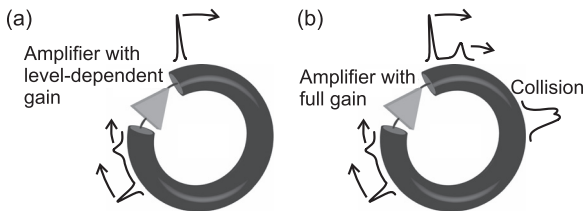

FIG. 3. (a) Level-dependent gain for stable, mode-locked dynamics. (b) Full gain for chaotic dynamics.

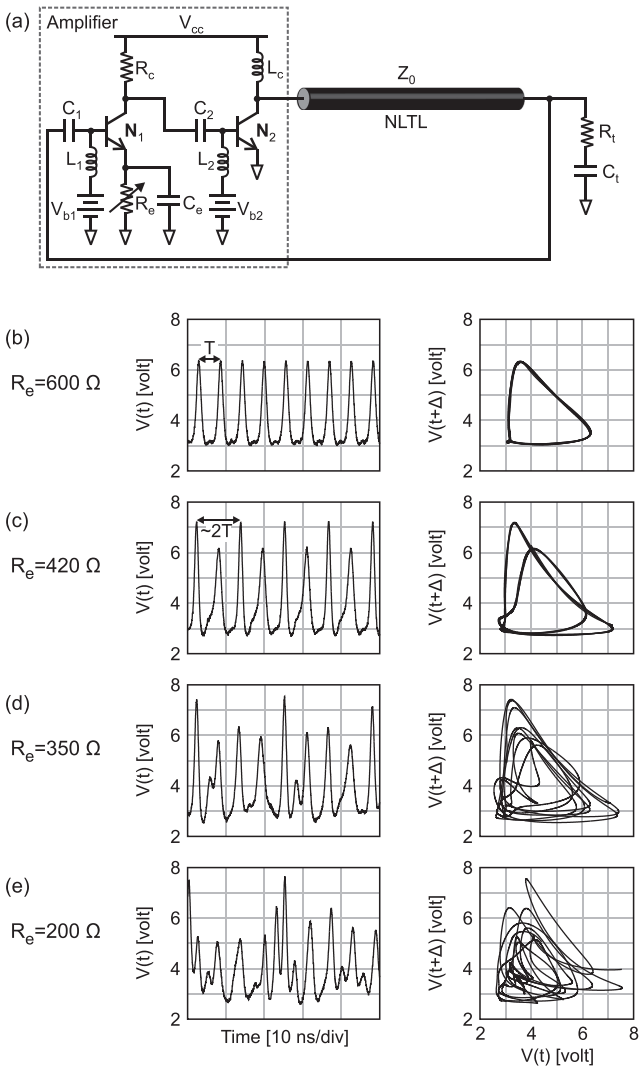

FIG. 4. (a) Oscillator that can be mode-locked or chaotic. (b)–(e) Measured $V(t)$ & phase-space trajectory for varying R_e.

large R_e, the *dc* average of the emitter voltage of $\mathbf{N}_1$ pulls up, thus small-amplitude inputs at the base of $\mathbf{N}_1$ are attenuated (level-dependent gain).[9–11] With a small R_e, the *dc* average of the emitter voltage of $\mathbf{N}_1$ pulls down, thus small-amplitude inputs at the base of $\mathbf{N}_1$ now can be amplified as well (full gain). This tunable first stage built around $\mathbf{N}_1$ is followed by the second stage based on transistor $\mathbf{N}_2$; since both stages invert the polarity of their respective inputs, the overall amplifier is non-inverting; this overall non-inversion is needed for mode-locked operation, while it does not matter for chaotic oscillation. The rest of capacitors and inductors in the amplifier are for biasing, decoupling, and loading.

The NLTL consists of 24 inductor-varactor sections. Each inductance is 40 nH. Each varactor, which is a reverse-biased *pn*-junction diode, has a nominal capacitance of 16 pF. The nominal characteristic impedance Z_0 of the NLTL is then 50 Ω. The NLTL is terminated with a resistor $R_t \sim Z_0$ and a decoupling capacitor C_t.

Figures 4(b)–4(e) show the measured voltage $V(t)$ at the middle of the NLTL for various values of R_e. We measure $V(t)$ with a real-time oscilloscope (sampling rate: 5 GS/s) in conjunction with an active high-impedance (100 kΩ) probe. For $R_e = 600$ Ω [Fig. 4(b)] with which level-dependent gain

firmly sets in, four tall, main, identical solitons circulate in the loop after the initial start-up, while small perturbations are suppressed. As a result, a periodic train of mode-locked solitons manifest in $V(t)$ with a pulse repetition period of $T = 5.7$ ns (if the transmission line is linear, sinusoidal oscillation will occur[22]). The corresponding 2-dimensional phase-space trajectory—$V(t+\Delta)$ vs. $V(t)$ with $\Delta = 1.2$ ns—is a one-loop limit cycle; $\Delta = 1.2$ ns is chosen via the standard prescription of the time-delay embedding method.[23]

With R_e reduced to 420 Ω [Fig. 4(c)], the threshold for the level-dependent gain is lowered. This allows not only the four main solitons but also four parasitic shorter solitons to circulate in the loop, where the speed of the shorter solitons is half of that of the taller ones. Thus, in $V(t)$, each tall pulse corresponds to a main soliton arriving at the measurement node, while each short pulse is the nonlinear joint effect of a main soliton and a shorter parasitic soliton colliding at the node. This interplay between the tall and short solitons signifies the period-doubling bifurcation that has occurred in reducing R_e from 600 Ω to 420 Ω. The bifurcation is also seen by comparing Figs. 4(c) to 4(b); the period of the former is approximately twice that of the latter (it is not exactly twice, as the amplifier delay and soliton amplitude/speed are altered with the changed R_e). Correspondingly, the phase-space trajectory in Fig. 4(c) makes two loops before closing.

As we further reduce R_e to 350 Ω [Fig. 4(d)] to further lower the threshold of the level-dependent gain, more parasitic solitons grow out of small perturbations, soliton collisions become prevalent, and an aperiodic waveform emerges. (Due to noise and lack of precise R_e control, we cannot resolve the infinite number of period-doubling bifurcations in going from Figs. 4(c) to 4(d).) This trend is intensified with further reduction of R_e to 200 Ω [Fig. 4(e)]; the amplifier now exhibits a full-gain characteristic, and $V(t)$ and phase-space trajectory now show characteristically chaotic oscillation.

Having demonstrated the route from mode-locked to chaotic oscillation via increased soliton collisions, we now move the focus to examining the nature of the chaotic signals. To this end, we construct a second, now always-chaotic, soliton oscillator at the discrete level [Fig. 5(a)]. Its amplifier is simplified (while the NLTL remains the same), for it does not have to incorporate the gain characteristic tuning; it just has a full-gain characteristic. Thus, the R_eC_e network from the previous amplifier is omitted. Also the second stage of the previous amplifier is removed, because whether the amplifier is inverting or non-inverting does not matter for chaos generation. The overall gain magnitude, however, is carefully adjusted via the inductance L_c (as in the previous amplifier in the chaotic mode), because the gain should be large enough for solitons to be sustained, but too large a gain would saturate the input signal into pulses of similar amplitudes, with which soliton collisions are difficult to achieve.

Figures 5(b) and 5(c) show the measured voltage $V(t)$ at the middle of the NLTL and its power spectrum with respect to 50 Ω. The aperiodic waveform and continuous spectral distribution indicate chaotic oscillation.

To further support that $V(t)$ is chaotic, we perform Lyapunov analysis.[24,25] A trajectory in a 6-dimensional phase space—$[V(t), V(t+\Delta), V(t+2\Delta),\ldots, V(t+5\Delta)]$ with $\Delta = 1.2$ ns—consisting of 261 600 points is considered

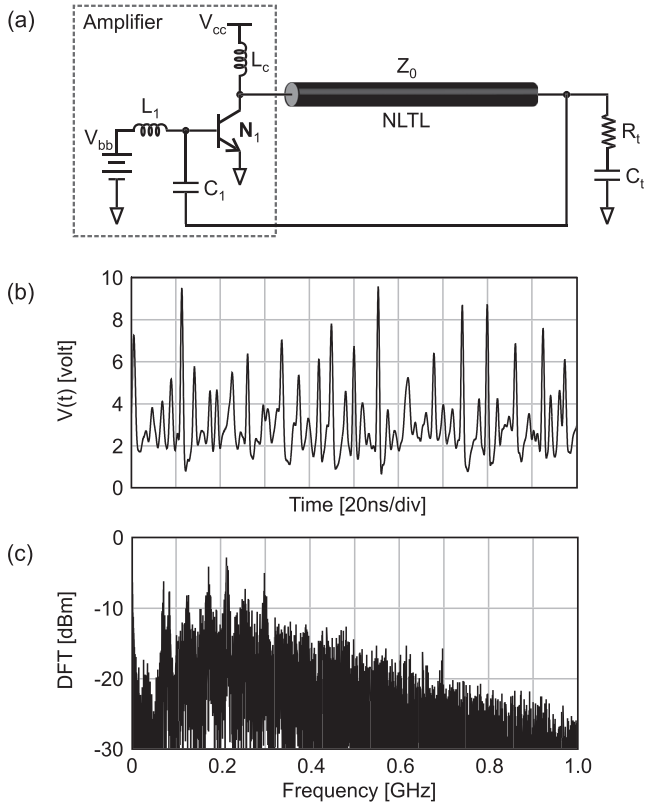

FIG. 5. (a) Chaotic soliton oscillator. (b) Measured waveform. (c) Its power spectrum with respect to 50 Ω.

(although the chaos has a higher dimensionality as seen shortly, the use of this lower dimensionality does not invalidate the Lyapunov analysis). Among all the 261 600 points comprising this trajectory, we choose a point and locate its nearest neighbor [P_0 and P_x, Fig. 6(a)] and consider two sub-trajectories starting from these two points. We then measure the time evolution of their distance [δ_0, δ_1, δ_2, … Fig. 6(a)]. The result is shown as the solid curve in Fig. 6(b), which shows that a pair of initially close sub-trajectories separate exponentially fast.

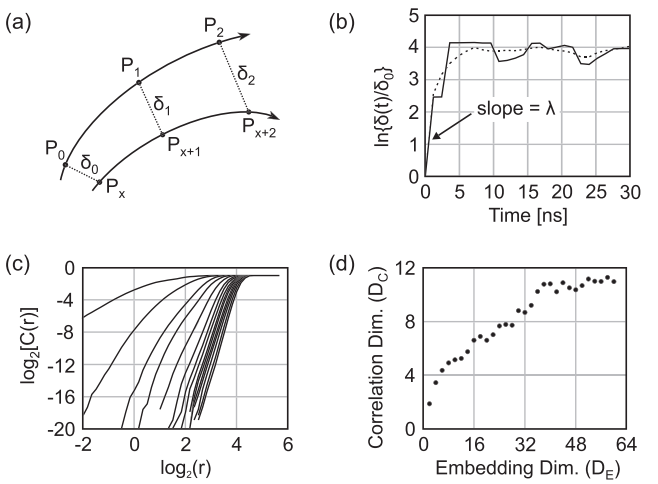

FIG. 6. (a) Two sub-trajectories. (b) Evolution of the distance between two initially close sub-trajectories. Solid: from a pair. Dashed: average from 200 pairs. (c) Correlation sum curves for varying D_E. (d) D_C vs. D_E.

We repeat the same analysis for 200 different pairs of initially close sub-trajectories (with each initial distance δ_0 smaller than 10 mV). The dashed curve in Fig. 6(b) is the averaged result; the initial positive slope of the curve, or the positive Lyapunov exponent λ, shows that two nearby sub-trajectories separate exponentially fast, i.e., $\delta(t) \approx e^{\lambda t}\delta_0$ (the curve eventually saturates, as the separation of two sub-trajectories grows comparable to the span of the overall phase portrait). This Lyapunov analysis along with the waveform and spectrum [Fig. 5] supports the chaotic nature of the oscillator.

To find the dimensionality of the chaos generated by the oscillator of Fig. 5(a), we perform analysis on the correlation dimension, D_C, following the well-established prescription.[26] Fig. 6(c) shows the correlation sum $C(r)$ as a function of r, the threshold distance in the reconstructed phase space. In Fig. 6(c), each curve is attained for a different embedding dimension D_E; the uppermost curve is for $D_E = 2$ and the rest of the curves are obtained by increasing D_E in steps of 4. As D_E increases, the slopes of the curves saturate to 11—see also Fig. 6(d)—from which we conclude $D_C \sim 11$. This high-dimensional chaos is due to the large number of energy storing elements (24 inductor-varactor pairs) in the NLTL. The measured dimensionality of 11 is less than the number of the relevant energy storing elements, because the voltages of neighboring varactors are correlated.

We have generated chaos by colliding solitons on the NLTL. While there exists a variety of chaotic circuits, the chaos generation principle demonstrated in this work can be particularly attractive for large-bandwidth applications, because of the high-speed nature of the NLTL, i.e., short soliton pulse duration on the NLTL;[27,28] integrated NLTLs using Schottky diode varactors have been shown to achieve a sub-picosecond pulse rise time.[27] Therefore, if our chaotic circuit is integrated and optimized for the speed reaching into the THz regime, it may be used as a ultrahigh-rate random number generator[5] and for high-bandwidth encrypted chaotic communication based on chaotic transmitter-receiver synchronization.[6–8] In this connection, it would be also interesting to extend this work into other types of THz wave propagation media, in particular, low-dimensional plasmonic media such as GaAs/AlGaAs quantum well and graphene,[29–33] where soliton propagation can be enabled by integrating varactor nonlinearity with the plasmonic media.

We thank Air Force Office of Scientific Research (FA9550-13-1-0211) and Office of Naval Research (N00014-13-1-0806) for support, and Xiaofeng Li, David S. Ricketts, and Eli Tziperman for discussions.

[1]L. O. Chua, C. W. Wu, A. Huang, and G. Zhong, IEEE Trans. Circuits Syst. Regul. Pap. **40**, 732 (1993).
[2]G. Chen and T. Ueta, *Chaos in Circuits and Systems* (World Scientific Publishing, 2002).
[3]T. Kapitaniak, L. O. Chua, and G. Zhong, IEEE Trans. Circuits Syst. Regul. Pap. **41**, 499 (1994).
[4]J. Suykens and L. O. Chua, Int. J. Bifurcation Chaos **7**, 1873 (1997).
[5]T. Stojanovski, J. Pihl, and L. Kocarev, IEEE Trans. Circuits Syst. Regul. Pap. **48**, 382 (2001).
[6]K. Cuomo and A. Oppenheim, Phys. Rev. Lett. **71**, 65 (1993).
[7]G. D. VanWiggeren and R. Roy, Phys. Rev. Lett. **81**, 3547 (1998).
[8]L. M. Pecora and T. L. Carroll, Phys. Rev. Lett. **64**, 821 (1990).
[9]D. S. Ricketts, X. Li, and D. Ham, IEEE Trans. Microwave Theory Tech. **54**, 373 (2006).
[10]D. S. Ricketts, X. Li, N. Sun, K. Woo, and D. Ham, IEEE J. Solid-State Circuits **42**, 1657 (2007).
[11]O. O. Yildirim, D. S. Ricketts, and D. Ham, IEEE Trans. Microwave Theory Tech. **57**, 2344 (2009).
[12]X. Li, O. Ozgur Yildirim, W. Zhu, and D. Ham, IEEE Trans. Microwave Theory Tech. **58**, 2105 (2010).
[13]M. Wu, B. A. Kalinikos, and C. E. Patton, Phys. Rev. Lett. **95**, 237202 (2005).
[14]L. M. Zhao, D. Y. Tang, F. Lin, and B. Zhao, Opt. Express **12**, 4573 (2004).
[15]D. J. Zheng, W. J. Yeh, and O. G. Symko, Phys. Lett. A **140**, 225 (1989).
[16]A. C. Scott, F. Y. F. Chu, and D. W. McLaughlin, Proc. IEEE **61**, 1443 (1973).
[17]N. Zabusky and M. Kruskal, Phys. Rev. Lett. **15**, 240 (1965).
[18]R. Hirota and K. Suzuki, Proc. IEEE **61**, 1483 (1973).
[19]M. Imada, J. Phys. Soc. Jpn. **52**, 1946 (1983).
[20]D. Ham, X. Li, S. Denenberg, T. H. Lee, and D. S. Ricketts, IEEE Commun. Mag. **44**, 126 (2006).
[21]T. Kawahara and S. Toh, *Nonlinear Wave Motion*, edited by A. Jeffrey (Longman, New York, 1989), Vol. 43, p. 95.
[22]W. Andress and D. Ham, IEEE J. Solid-State Circuits **40**, 638 (2005).
[23]A. Tsonis, *Chaos: From Theory to Applications* (Plenum Press, 1992).
[24]S. H. Strogatz, *Nonlinear Dynamics and Chaos* (Westview Press, 1994).
[25]A. Wolf, J. B. Swift, H. L. Swinney, and J. A. Vastano, Physica D **16**, 285 (1985).
[26]P. Grassberger and I. Procaccia, Phys. Rev. Lett. **50**, 346 (1983).
[27]W. van der Weide, Appl. Phys. Lett. **65**, 881 (1994).
[28]M. Rodwell, S. Allen, R. Yu, M. Case, M. Reddy, E. Carman, J. Pusl, M. Kamegawa, Y. Konishi, and R. Pullela, Proc. IEEE **82**, 1037 (1994).
[29]H. Yoon, C. Forsythe, L. Wang, N. Tombros, K. Watanabe, T. Taniguchi, J. Hone, P. Kim, and D. Ham, "Measurement of Collective Dynamical Mass of Dirac Fermions in Graphene," e-print arXiv:1401.4240.
[30]K. Yeung, J. Chee, H. Yoon, Y. Song, J. Kong, and D. Ham, Nano Lett. **14**, 2479 (2014).
[31]W. Andress, H. Yoon, K. Yeung, L. Qin, K. West, L. Pfeiffer, and D. Ham, Nano Lett. **12**, 2272 (2012).
[32]K. Yeung, H. Yoon, W. Andress, K. West, L. Pfeiffer, and D. Ham, Appl. Phys. Lett. **102**, 021104 (2013).
[33]H. Yoon, K. Yeung, V. Umansky, and D. Ham, Nature **488**, 65 (2012).